European Journal of Pharmacology 1011 (2026) 178436

Contents lists available at ScienceDirect

European Journal of Pharmacology

journal homepage: www.elsevier.com/locate/ejphar

Uncovering the pleiotropic effects of oleoylethanolamide on obesity-driven chronic kidney disease in mice

Federica Comella [a], Stefania Melini [a], Nicola Opallo [a], Evaristo Di Napoli [b], Nicole Pia Navatti [a], Orlando Paciello [b], Maria Carmela Ferrante [b], Rosaria Meli [a], Giuseppina Mattace Raso [a,*], Claudio Pirozzi [a]

[a] Department of Pharmacy, School of Medicine, University of Naples Federico II, 80131 Naples, Italy
[b] Department of Veterinary Medicine and Animal Productions, University of Naples Federico II, 80137, Naples, Italy

ARTICLE INFO

Keywords:
High-fat diet
Glucose transporters
Lipotoxicity
Inflammation
Human epithelial tubular cells (HK-2)
Mitochondrial bioenergetics

ABSTRACT

Metabolic alterations, resulting from obesity, drive chronic kidney disease (CKD) through mechanisms including lipotoxicity, inflammation, and fibrosis. Oleoylethanolamide (OEA), an endogenous compound belonging to the N-acylethanolamine family, has been widely studied for its metabolic properties. However, emerging evidence highlights its anti-inflammatory and anti-fibrotic effects. Here, we explored the effect of OEA on high-fat diet (HFD)-induced renal damage associated with obesity in mice.

OEA treatment improved kidney function by restoring urine output and reducing proteinuria and albuminuria in obese mice. Moreover, OEA normalized serum creatinine and blood urea nitrogen levels, which were altered by HFD feeding, and decreased the transcription of kidney injury molecule-1 and neutrophil gelatinase-associated lipocalin, associated with renal damage. OEA also counteracted renal glucose dysmetabolism by reducing glycogen content and modulating the protein expression of glucose transporters. Furthermore, OEA exerted marked anti-inflammatory and antifibrotic effects in kidney, further confirmed by a reduction in the transcription of pro-inflammatory and pro-fibrotic markers. OEA reduced renal steatosis, improving lipid metabolism through increased peroxisome proliferator-activated receptor-α and fibroblast growth factor 21 transcription and reduced triglyceride trafficking by the downregulation of diacylglycerol O-acyltransferase 1. Finally, to highlight the direct effect of OEA in the kidney, we confirmed its protective activity against lipotoxicity and demonstrated its ability to improve mitochondrial bioenergetics in human proximal tubular epithelial cells (HK-2).

These results indicate that OEA may be a promising therapeutic molecule for restraining CKD-related alterations associated with obesity and metabolic disorders.

1. Introduction

Chronic overconsumption of hypercaloric diets with high content of carbohydrates and/or fat is related to metabolic alterations, possibly leading to obesity, insulin resistance, dyslipidemia, and hypertension. As known, the prolonged metabolic imbalance of circulating lipids from endogenous and exogenous sources leads to ectopic fat accumulation also in the peripheral organs other than adipose tissues, including the kidney. Renal lipid accumulation, deriving from the imbalance between fatty acid inflow and utilization, exerts a direct detrimental effect, promoting local lipotoxicity, oxidative stress, fibrosis, and inflammation, molecular events leading to glomerular and tubule-interstitial

Abbreviations: (PPAR)-α, peroxisome proliferator activating receptor; (HFD), High-fat diet; (OEA), Oleoylethanolamide; (GLUT)2, Glucose transporter; (SGLT)2, Sodium-glucose transporter; (IL), Interleukin; (TGF-β1), Transforming growth factor beta 1; (NAE), N-acyl ethanolamine; (ORO), Oil red O; (HK-2), Human epithelial tubular cells; (DGAT), Diacylglycerol O-Acyltransferase; (CKD), Chronic kidney disease; (UACR), Urinary albumin and creatinine ratio; (H&E), Hematoxylin and eosin; (PAS), Periodic acid – Schiff; (NGAL), Neutrophil gelatinase-associated lipocalin; (BUN), blood urea nitrogen; (MCP), Monocyte chemoattractant protein; (Nfkb), Nuclear factor kappa beta subunit; (KIM), Kidney injury molecule; (Tlr), Toll-like receptor; (PAL), Palmitate; (FAS), Fatty acid synthase; (FGF)21, Fibroblast growth factor; (ROS), Reactive oxygen species.

* Corresponding author. Department of Pharmacy, Via Domenico Montesano, 49, 80131, Naples, Italy.
E-mail address: mattace@unina.it (G. Mattace Raso).

https://doi.org/10.1016/j.ejphar.2025.178436
Received 20 June 2025; Received in revised form 26 November 2025; Accepted 2 December 2025
Available online 4 December 2025

damage (Ren et al., 2023).

Obesity-induced kidney injury, compared to other obesity-related comorbidities, has a faster progression towards chronic kidney disease (CKD). Very recent reports have concluded that CKD is predicted to become a major global health issue within this century (Francis et al., 2024); therefore, early diagnosis and interventions are advocated to control morbidity and mortality, disability, reduced quality of life and other psychosocial harms associated with it. Since obesity constitutes a predominant risk factor for the onset and progression of CKD (Kounatidis et al., 2024), among the so-called primordial preventions of CKD, even more upstream than the primary strategies, there is the management and therapy of obesity (Kalantar-Zadeh and Li, 2020), whose current options have been recently reviewed and evaluated through a kidney-oriented lens (Taber-Hight et al., 2024).

Peroxisome proliferator-activated receptor (PPAR)-α, is a central regulator of fatty acid metabolism, thereby accelerating fatty acid metabolism and reducing fat accumulation. Notably, this receptor is abundantly expressed in the proximal tubules and medullary thick ascending limbs and to a lesser extent, in glomerular mesangial cells (Guan, 2002; Kamijo et al., 2002), indicating its critical involvement in maintaining the renal balance of energy production and consumption. Meanwhile, PPAR-α has also been demonstrated to exert profound anti-inflammatory and antifibrotic activity (Chung et al., 2018; Comella et al., 2024b; Impellizzeri et al., 2014; Mattace Raso et al., 2013; Yang et al., 2015), implying to be a link between lipid metabolism and inflammation control. Although PPAR-$\alpha^{-/-}$ mice did not show kidney disease, they are more prone to both acute and chronic kidney injury following different challenges, and on the other hand, transgenic expression of PPAR-α, in tubule cells protected mice against acute and chronic kidney disease (Lee et al., 2024; Li et al., 2009). Concomitantly, PPAR-α deficiency worsened the severity of diabetic nephropathy (Park et al., 2006).

Oleoylethanolamide (OEA), a lipid mediator belonging to the N-acylethanolamines (NAEs) family, has been demonstrated to have a role in appetite and body weight control. These effects are mainly attributed to the activation of PPAR-α, even if other mechanisms could be involved in the OEA regulation of energy homeostasis and appetite control (Laleh et al., 2018). On the other hand, several reports have indicated that OEA possesses anti-inflammatory and anti-fibrotic effects (Chen et al., 2015; Pontis et al., 2016). Meanwhile, we have also found that OEA counteracted the transition of acute kidney injury into CKD, limiting the inflammatory and fibrotic process, via PPAR-α activation since OEA failed to exert its beneficial activity in PPAR-$\alpha^{-/-}$ mice (Comella et al., 2024b).

The "dual" ability of OEA to control weight gain, alongside its nephroprotective effect, makes this molecule as an attractive candidate for further investigation in kidney injury linked to metabolic alterations. Accordingly, we aimed to investigate the effects of OEA on CKD induced by high-fat diet (HFD) feeding in mice, with a particular focus on its involvement in controlling inflammatory and fibrotic processes, as well as regulating metabolism.

2. Methods

2.1. Ethical statement

Animal care and experimental procedures were carried out in compliance with International and National Law and Policies and approved by the Local Animal Care Office (Centro Servizi Veterinari, Università degli Studi di Napoli, Federico II, ITA) and the Italian Ministry of Health under protocol no. 1210/2020-PR. Animal studies were performed in compliance with the Italian D.L. (No. 26 of 4 March 2014) of the Italian Ministry of Health and the EU Directive 2010/63/EU for animal experiments, ARRIVE guidelines, and the Basel declaration, including the 3Rs concept.

2.2. Animals and treatments

6-week-old male C57BL/6J mice were obtained from Charles River Laboratories Italia S.r.l. and housed in stainless steel cages under controlled conditions of room temperature (RT) (22 ± 1 °C) and illumination (12:12 h light-dark cycle). Mice were maintained with *ad libitum* access to a diet and tap water. The animals were allowed to acclimatize for one week. Then they were randomly divided into three groups (n=8–10) as reported below: (i) control group (STD) receiving chow standard diet and vehicle (water/PEG/TWEEN 80 (90/5/5 v/v)); (ii) HFD group receiving vehicle; (iii) HFD group intraperitoneally treated with OEA (HFD + OEA) at a dose of 2,5 mg/kg/die for 8 weeks. The OEA dose, selected on previous study (Comella et al., 2024a) was validated through animal-to-human dose conversion using standard allometric scaling method based on body surface area (Freireich et al., 1966). The standard chow diet had 17 % fat without sucrose, while HFD had 45 % energy derived from fat and 7 % sucrose (D12451, Research diet, USA). OEA was resuspended in water/PEG/TWEEN 80 (90/5/5 v/v). Treatments started after 12 weeks of HFD feeding and were conducted concurrently with the HFD. At the end of the experiment, all mice were anaesthetized with enflurane by inhalation and euthanized, followed by cervical dislocation. Blood was collected from all animals by cardiac puncture and was centrifuged at 2500 rpm at 4 °C for 12 min to obtain the serum samples. Then, kidneys were collected, snap-frozen and stored at −80 °C for subsequent analysis.

2.3. Metabolic cages

Mice from all groups were placed individually in metabolic cages (41700-003, Ugo Basile, ITA) the day before the sacrifice. This procedure allows for monitoring of water intake by weighing the water dispenser at the beginning and end of the 24 h experiment. In addition, urinary output for 24 h was evaluated, and urine samples were collected for functional measurements.

2.4. Serum and urine analysis

Urea and creatinine levels were measured in serum samples. Urea was expressed as blood urea nitrogen (BUN), obtained by dividing the urea concentration in the blood by 2.14 (reflecting the ratio between the molecular weight of urea and urea nitrogen). The formula is BUN = [urea]/2.14. These parameters were quantified using commercially available following the manufacturer's instructions. To minimize intra-test variation, all samples and standards were analyzed in duplicate. Moreover, we evaluated urine albumin levels using an ELISA kit (ab207620, Abcam, UK). Creatinine level was also determined in the urinary sample and urine albumin and creatinine data were used to calculate the ratio of urinary albumin and creatinine (UACR) excretion, which is a measure of the kidney injury. Proteinuria was quantified using the Bradford assay, a colorimetric method for protein measurement in urine samples. Absorbance was recorded at 595 nm using a spectrophotometer, and protein concentration was determined based on a standard curve generated from the absorbance values of the samples.

2.5. Histological scores analysis

Kidneys were removed, fixed in neutered buffered formalin, and embedded in paraffin. Kidney sections were stained with Hematoxylin and Eosin (H&E), Periodic acid–Schiff (PAS), and Masson's Trichrome stains. Inflammation and steatosis were scored on a scale of 0 (no steatosis), 1 (mild, 1 < 30 %), 2 (moderate, 30–70 %) and 3 (severe, >70 %). The positive PAS reaction highlighted the variable amount of glycogen within the affected renal cells with a magenta red colour. Masson's positive Trichrome reaction showed purple nuclei with hematoxylin, cytoplasm in vivid red, and connective tissue strongly stained in blue. The PAS and Masson's Trichrome reactions were scored

into grades (0 negative; 1 slightly positive; 2 moderately positive; 3 positive).

2.6. Immunohistochemical analysis

Mouse kidneys were fixed in 10 % neutral-buffered formalin, processed, and embedded in paraffin. Serial 3 μm sections were used for immunohistochemical evaluation. Immunohistochemistry was performed according to our established protocol (De Biase et al., 2024; Dimatteo et al., 2024; Vaccaro et al., 2024). Briefly, kidney tissue sections were deparaffinized and rehydrated through graded alcohols. Endogenous peroxidase was quenched by incubation in 0.3 % H_2O_2 in methanol (4:1) for 15 min. Heat-induced epitope retrieval was carried out in citrate buffer (pH 6.0) using microwave heating, followed by cooling to room temperature and rinsing in PBS (pH 7.4, 0.01 M). Immunolabeling was performed using the MACH1 Universal HRP-Polymer Detection Kit (Code M1U539 G, L10; Bio-Optica, Milan, Italy), following the manufacturer's instructions. Sections were incubated overnight at 4 °C with a rabbit monoclonal anti-α-smooth muscle actin antibody (Cell Signaling Technology, Danvers, MA, USA; clone D4K9N) diluted 1:200 in PBS. Signal was developed with DAB, and nuclei were counterstained with hematoxylin; slides were then dehydrated and mounted. Negative controls consisted of sections processed in parallel with the omission of the primary antibody. As positive controls, mouse spleen sections were included in each run. Vascular smooth muscle within the kidney served as an internal positive control. For image acquisition, ten non-overlapping 20× fields per case were randomly selected and digitized using the Pannoramic II scanner (3DHISTECH, Budapest, Hungary). α-SMA immunoreactivity in the tubulo-interstitial compartment (excluding vascular media and glomerular arterioles) was assessed by two independent, blinded pathologists and expressed using a semi-quantitative score: 0 = absent; 1 = mild (<5 % of field area); 2 = moderate (5–15 %); 3 = marked (>15 %). At least 10 HPF (0.237 mm^2; 40× objective, 10× ocular, field number 22 mm) were evaluated per sample. Discrepancies were resolved by consensus.

2.7. Cell culture

The human proximal tubular cell line (HK-2) was purchased from the American type culture collection (ATCC, CRL-2190™, Manassas, VA) and cultured according to ATCC guidelines. HK-2 cells were grown in DMEM 1.0 g/L glucose (GIBCO, Thermo Fisher Scientific, USA, Cat #31885023) supplemented with 10 % FBS (GIBCO, Thermo Fisher Scientific, USA, Cat #10270106), Penicillin-Streptomycin (5000 U/mL) (GIBCO, Thermo Fisher Scientific, USA, Cat #15070063) and maintained at 37 °C in a 5 % CO_2 incubator. All cultures used in the experiment were between passages 22 and 30.

2.8. Oil Red O staining

Cells were seeded in P6-well plates, when cells reached 60–70 % of confluence, the medium was replaced with 2 % FBS in DMEM. After 6 h starvation, cells were incubated for 24 h with palmitate (PAL) 200 μM, (Sigma-Aldrich, USA Cat #P9767). 1 h before the challenge, cells were pretreated with OEA (5 μM). Cells were first washed in PBS and subsequently fixed with paraformaldehyde (10 %) for 1 h. Then, the cells were washed with distilled water and incubated with 60 % Oil Red O (ORO) (#O9755, Sigma-Aldrich) (prepared by dissolving 0.5 g of ORO in 100 ml of isopropanol) for 2 h, followed by washing with PBS. The cells were visualized using a Zeiss AXIO observer microscope. For quantification, the cells were subsequently incubated with isopropyl alcohol for 10 min. The solution was transferred to a 96-well plate and absorbance was measured at 550 nm using a spectrophotometer.

2.9. Western blotting

The kidney was homogenized in lysis buffer (20 mM Tris–HCl, pH 7,5, 10 mM NaF, 150 mM NaCl, 1 % Nonidet P-40, 1 mM phenylmethylsulphonyl fluoride, 1 mM Na_3VO_4, leupeptin 10 μg/mL, and trypsin inhibitor 10 μg/mL) with a homogenizer (Ultra-Turrax T8; IKA Labortechnik, DEU). Total protein lysates were obtained as supernatant by centrifugation at 14,000×*g* for 15 min at 4 °C. Protein concentrations were estimated by the Bio-Rad protein assay using free bovine serum albumin (BSA) as standard. An equal amount of protein (40 μg) was subjected to SDS-PAGE and electro-transferred onto a nitrocellulose membrane using a Bio-Rad Transblot (Bio-Rad, Milan, Italy). The following parameters were set: 10 min of blotting time, 1.3 mA (approximately 25 V). The membrane was then blocked with 1X phosphate buffer solution (PBS) and 5 % non-fat dried milk for 45 min at RT and was incubated with rabbit polyclonal antibodies against glucose transporter (GLUT)-2 (1:1000; Cat) and sodium-glucose cotransporter (SGLT)2 (1:1000; Santa Cruz Biotechnology, Cat#sc-393350). Anti-β-actin (1:5000; Sigma-Aldrich Cat #A5441) was used to normalize and ensure equal sample loading. Visualization of protein band intensities was determined by chemiluminescence using ChemiDoc MP Imaging System (Bio-Rad Laboratories, Inc, USA). Densitometric analysis of the protein bands was performed using Image Lab software (Bio-Rad Laboratories, version 6.1). Band intensities were expressed in arbitrary units (A.U.) and normalized to the corresponding housekeeping protein (β-actin) to account the loading variability. To ensure consistency and comparability all samples were analyzed under identical exposure conditions.

2.10. Real-time PCR analysis

Total RNA was isolated from the kidney and HK-2 cells using TRIzol Reagent (Bio-Rad Laboratories, USA) through the NucleoSpin kit (Macherey-Nagel cod.740955.50), according to the manufacturer's instructions. The quality and quantity of total RNA were measured using a NanoDrop One spectrophotometer (Thermo Fisher Scientific, USA). RNA samples with a 260/280 ratio between 2.0 and 2.2 were considered qualified. cDNA was obtained using a High-Capacity cDNA Reverse Transcription Kit (cod. 4374966, Thermo Fisher Scientific, USA) from 8 μg of total RNA. PCRs were performed on the Bio-Rad CFX96 Connect Real-time PCR System instrument and software (CFX Maestro Software). PCR conditions were 15 min at 95 °C followed by 40 cycles of two-step PCR denaturation at 94 °C for 15 s, annealing extension at 55 °C for 30 s and extension at 72 °C for 30 s. Each sample contained 500 ng of cDNA in 2X QuantiTect SYBR Green PCR Master Mix (cod. 204145, Qiagen, DEU) and primers pairs to amplify mouse kidney injury molecule (KIM)-1 (*Havcr1*), neutrophil gelatinase-associated lipocalin (NGAL) (*Lcn2*), phosphoenolpyruvate carboxykinase (PCK)1 (*Pck1*), TNF (*Tnf*) interleukin (IL)-1β (*Il1b*), IL-6 (*Il6*), chemokine (C-C motif) ligand 2 also referred as monocyte chemoattractant protein (MCP)1 (*Ccl2*), hormone receptor-like 1 (*Emr1*), also known as F4/80, nuclear factor kappa beta subunit 1 (*Nfkb1*), toll-like receptor 4 (*Tlr4*), PPAR-α (*Ppara*), Fibroblast Growth Factor (FGF)21 (*Fgf21*), diacylglycerol O-acyltransferase (DGAT)1 (*Dgat1*), transforming growth factor beta (TGF-β)1 (*Tgfb1*), fibronectin 1 (*Fn1*), collagen type IV alpha 1 chain (*Col4a1*), fatty acid synthase (FAS) (*Fasn*), Cluster of Differentiation (CD)36 (*Cd36*) (Qiagen, DEU) in a final volume of 50 μl. The relative amount of each studied mRNA was normalized to *Gapdh* or *18s* as a housekeeping gene (Qiagen, DEU) (Table S1), and data were analyzed according to the $2^{-\Delta\Delta CT}$ method.

2.11. Measurement of reactive oxygen species (ROS)

ROS levels in kidney tissue were assessed as previously described (Pirozzi et al., 2020). Briefly, freshly prepared kidney homogenates were incubated with 5 μM dichlorofluorescein diacetate (DCFH-DA; cat. no.

35845, Sigma–Aldrich, Milan, Italy) dissolved in dimethyl sulfoxide (DMSO, cat. no. D5879, Sigma–Aldrich, Milan, Italy) for 15 min at 37 °C. Samples were then centrifuged at 12,500×*g* for 10 min at 4 °C. The resulting pellet was resuspended in 5 mL of 100 mM potassium phosphate buffer (pH 7.4) and incubated for an additional 60 min at 37 °C to allow ROS-mediated oxidation of DCFH-DA to the fluorescent DCF.

HK-2 cells were seeded in 96-well plates (Lumox® multiwell, Sarstedt, Cat. No. 94.6120.096; Nürnbrecht, Germany) at a density of 3×10^4 cells per well and allowed to adhere overnight. After a 6 h serum starvation period, cells were exposed to PAL (300 μM) for 4 h. One hour before PAL treatment, cells were pre-treated with OEA (5 μM). ROS levels were assessed using 10 μmol/L DCFH-DA, diluted in serum- and phenol red-free DMEM. The dye solution was added directly to each well, and cells were incubated in the dark at 37 °C with 5 % CO_2 for 20 min. Following incubation, cells were washed three times with PBS to remove excess dye.

Fluorescence intensity was measured using a Promega GloMax Explorer Microplate Reader (cat. no. GM3560, Milan, Italy) at excitation and emission wavelengths of 488 nm and 525 nm, respectively. ROS levels were quantified based on a dichlorofluorescein standard curve (0–1 mM) prepared in DMSO. Fluorescence readings were normalized to protein concentration determined by the Bradford assay and expressed as fold change relative to control samples.

2.12. Cellular oxygen consumption measurement

Oxygen consumption rate (OCR), a measurement of mitochondrial respiration, was determined in the presence of specific mitochondrial activators and inhibitors. Oligomycin (ATP synthase blocker) was used to measure ATP turnover and to determine proton leak. Mitochondrial uncoupler FCCP (carbonyl cyanide 4-[trifluoromethoxy] phenylhydrazone) was used to measure maximum respiratory function (maximal OCR). Reserve capacity was calculated as a maximal OCR minus the basal respiration. Rotenone (inhibitor of complex I) and antimycin A (a blocker of complex III) were injected to completely shut the mitochondrial respiration down to confirm that any observed changes in respiration were mitochondrial (Brand and Nicholls, 2011; Dranka et al., 2011). We performed preliminary titration experiment using two different cell densities (15,000 and 30,000 cells/well) to obtain the optimal OCR range (100–200 pmol/min). Based on these results, we selected 15,000 cells/well as the optimal seeding density for subsequent analysis. After 6 h starvation, cells were incubated for 24-h with palmitate (PAL) 200 μM, (Sigma-Aldrich, USA Cat #P9767). 1 h before the challenge, cells were pretreated with OEA (5 μM). One day before the extracellular flux measurement, HK-2 cells were seeded at 15,000 cells per well in 24-well assay plates. 1 h before the experiment, the growth medium was removed, cells were washed and then incubated in a low buffered assay medium (Seahorse XF DMEM medium, pH 7.4, 103575-100 Agilent Technologies) supplemented with 1 mM pyruvate (103578-100), 2 mM glutamine (103579-100), and 10 mM glucose (103577-100). The plates were then assayed in the XFe24 analyzer. For a measurement of steady basal respiration, 4–5 measurements were taken before injecting ATP synthase inhibitor oligomycin at 1,5 μM (final concentration). Mitochondrial membrane uncoupler FCCP was then injected at 1 μM. Finally, a mixture of rotenone and antimycin A (0,5 μM) was injected. Mitochondrial basal respiration, proton leak, ATP-production coupled respiration, maximal respiration and spare capacity were measured. OCR rate was presented as pmoles O_2/min.

2.13. Data and statistical analysis

All experimental data are presented as the mean ± Standard Error of the Mean (SEM) of at least 5 individual measurements per group, with n defined as independent animal individuals. Shapiro-Wilk normality test was performed on all analyzed data. *In vitro* data are presented as the mean ± SEM from three different experiments in duplicate. They are also subjected to one-way variance analysis (ANOVA) for multiple comparisons, followed by Bonferroni's post hoc test, using GraphPad Prism 10 (GraphPad Software Inc., USA). Differences among groups were considered significant at values of $p < 0.05$.

3. Results

3.1. OEA recovers kidney function perturbed in obese mice

HFD feeding has been shown to induce obesity and metabolic syndrome in mice, along with renal damage and morphological alterations in the kidney (Ruggiero et al., 2011; Wei et al., 2004). Therefore, mice were fed an HFD (45 % kcal fat) for 20 weeks; from week 12 onward, when obesity was established, mice received OEA until week 20. Under these experimental conditions, OEA limited the increase in body weight, reduced fat mass, and improved systemic metabolic profile in HFD-fed mice (Supplementary data). As expected, long-term HFD feeding resulted in impaired kidney function, as evidenced by reduced water intake (Fig. 1A) and urine output (Fig. 1B) compared to the STD group, whereas OEA treatment restored these parameters. HFD-induced kidney dysfunction was further confirmed by alterations in proteinuria (Fig. 1C), 24 h urinary albumin levels (Fig. 1D) and the urinary albumin-to-creatinine ratio (UACR) (Fig. 1E), which were significantly improved in OEA-treated mice. The nephroprotective effect of OEA was further assessed by evaluating key serum markers of kidney function, including serum creatinine and BUN. HFD-fed mice exhibited elevated creatinine levels (Fig. 2A) compared to the STD group, which were significantly reduced following OEA treatment. Similarly, BUN levels (Fig. 2B) were significantly lower in OEA-treated mice than in HFD ones. Additionally, OEA treatment decreased the renal expression of tubular injury markers, such as *Havcr1* (Fig. 2C) and *Lcn2* (Fig. 2D), which were elevated in HFD-fed mice.

3.2. OEA reduces kidney pathological damage and glycogen deposition in HFD-fed mice

PAS staining revealed glycogen accumulation in the glomeruli and significant thickening of the basement membrane in the HFD group compared to the STD group (Fig. 3A). In contrast, the OEA-treated mice showed reduced glycogen accumulation and notable thinning of the basement membrane (Fig. 3B). These findings suggest that OEA effectively mitigates renal pathological damage and glycogen buildup induced by a HFD in mice. PCK1, a cytosolic enzyme essential for normal tubular function and glucose homeostasis, plays a key role in CKD progression (Verissimo et al., 2023). OEA treatment reduced *Pck1* mRNA expression that was markedly altered in the kidneys of HFD-fed mice (Fig. 3C). Additionally, we assessed the expression of key glucose transporters involved in renal glucose homeostasis. OEA treatment led to a slight reduction of GLUT2 (Fig. 3D) and a significant reduction of SGLT2 protein expression (Fig. 3E).

3.3. OEA attenuates the inflammatory process induced by HFD

H&E staining was performed to evaluate structural abnormalities in the kidney. As shown in Fig. 4A, the control group displayed an intact glomerular structure with no mesangial cell proliferation. In contrast, the HFD group exhibited excessive proliferation of mesangial cells and abnormal glomerular enlargement. Notably, in the OEA-treated group, glomerular morphology was restored, with significant improvement in both inflammation (Fig. 4B) and steatosis score (Fig. 4C).

To further assess the impact of OEA on renal cell recruitment and inflammation in response to HFD, we measured the mRNA expression levels of IL-1β, IL-6, TNF-α, MCP-1 and macrophage marker F4/80 in the kidney tissue (Fig. 4D). RT-PCR analysis revealed a marked upregulation of these inflammatory markers in the kidneys of HFD-fed mice, which were significantly reduced following OEA treatment. HFD feeding

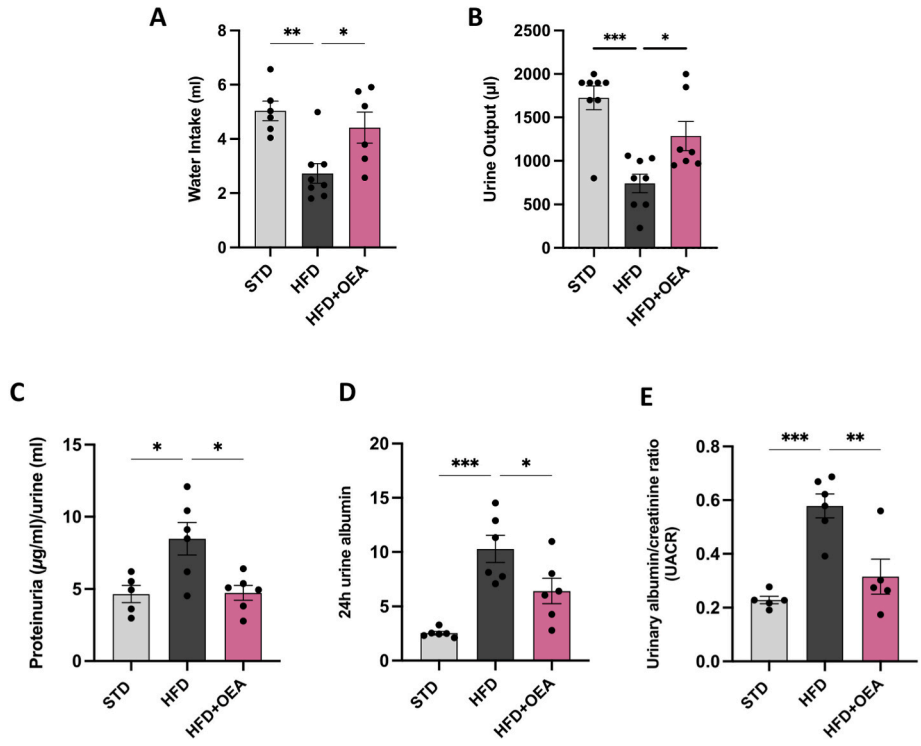

Fig. 1. OEA treatment preserves kidney function altered by HFD. Water intake (A) and urine output (B) are evaluated at the end of the experimental period. Proteinuria (C), 24-h urine albumin (D) and urinary albumin/creatinine ratio (UACR) (E) are measured. Results are shown as mean ± S.E.M (n= 5–8 each group) (*P < 0,05, **P < 0,01, and ***P < 0,001).

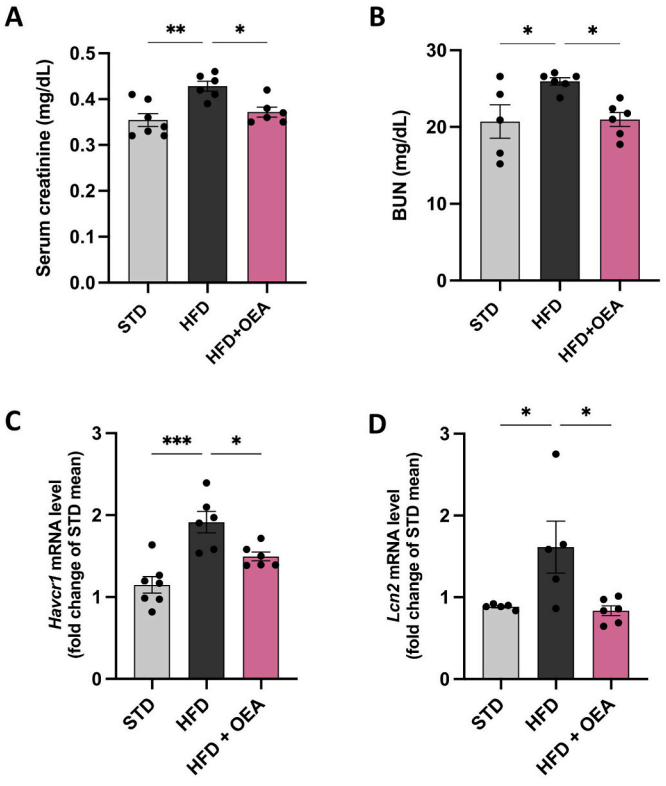

Fig. 2. OEA normalizes kidney parameters. Serum levels of kidney function markers, creatinine (A) and BUN (B) are evaluated. The mRNA expression of molecular markers of tubular injury, such as *Havcr1* (C) and *Lcn2* (D), is determined in kidney tissue. Results are shown as mean ± S.E.M (n= 5–7 each group) (*P < 0,05, **P < 0,01, and ***P < 0,001).

strongly induced the transcription of TLR4 and NF-κB in kidney tissue compared to the STD group, whereas OEA treatment reduced their expression (Fig. 4D). Next, oxidative stress was assessed by measuring ROS production in kidney tissue. The increased ROS production in the kidney of HFD mice was blunted by OEA treatment (Fig. 4E). Finally, given the reduced renal steatosis grade, we measured the mRNA levels of PPAR-α (Fig. 4F) and FGF21 (Fig. 4G), both of which were impaired in HFD-fed mice but restored upon OEA treatment. Contextually, OEA reduced the transcription of *Dgat1*, markedly altered by HFD feeding (Fig. 4H), suggesting a protective role against HFD-induced renal triglyceride accumulation and damage.

3.4. OEA treatment limits renal fibrotic response in obese mice

Masson's trichrome staining revealed that OEA treatment significantly reduced HFD-induced tubulointerstitial fibrosis. Obese mice exhibited a greater number of collagen-positive staining areas (Fig. 5A) and a higher fibrosis score (Fig. 5B) compared to control mice. Immunohistochemistry for α-SMA (Fig. 5C) showed a clear increase in the kidney of HFD mice, with continuous perivascular and peritubular stromal bands and bundled myofibroblast-like profiles, compared to the minimal staining found in the STD group, restricted to the vascular media and thin interstitial septa, with tubular epithelium remaining negative. In contrast, OEA blunted the HFD-associated increase in α-SMA–positive area, with a visible reduction in both extent and signal intensity compared with untreated HFD group, consistent with a partial attenuation of interstitial fibrosis. These findings were confirmed by the relative intensity score (Fig. 5D). To further investigate the antifibrotic effects of OEA, we analyzed the gene expression of TGF-β1 (Fig. 5E), a key regulator in renal fibrosis pathogenesis, along with two major extracellular matrix components, collagen type IV (Fig. 5F) and fibronectin (Fig. 5G). Their expression levels were significantly elevated in obese mice but markedly reduced following OEA treatment.

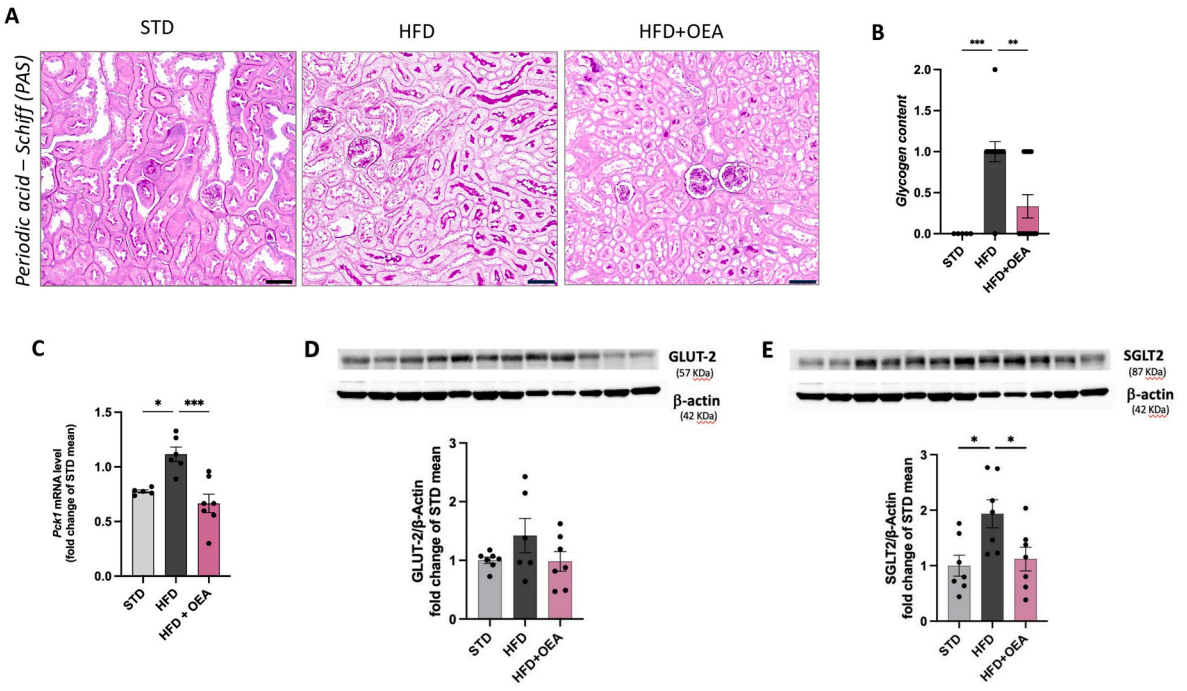

Fig. 3. OEA counteracts glycogen deposition induced by HFD. Representative photomicrographs of PAS-stained kidney sections (original magnification 200×) (A) and their relative glycogen content score (B) are shown. The mRNA transcription of *Pck1* (C) and the protein expression of GLUT2 (D) and SGLT2 (E) are assessed in the kidneys. Results are shown as mean ± S.E.M (n= 5–8 each group) (*P < 0,05, **P < 0,01 and ***P < 0,001).

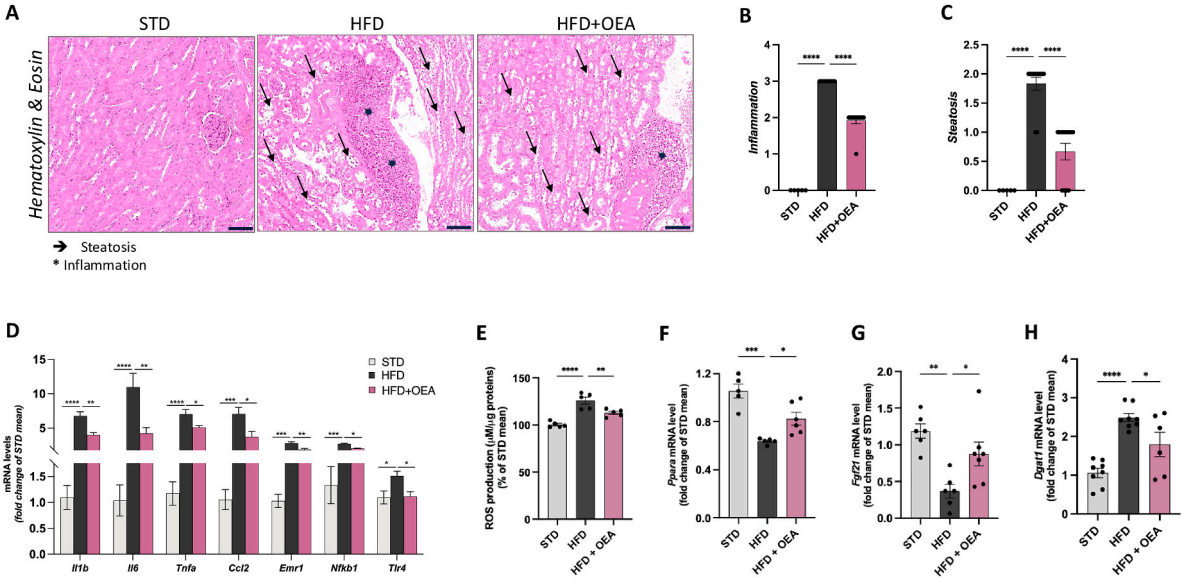

Fig. 4. OEA moderates the inflammatory responses in obese mice. Representative photomicrographs of H&E-stained kidney sections (original magnification 200×) of the STD, HFD and HFD + OEA group with micro and macrovacuolization (arrow) and inflammatory cells (asterisk) are displayed (A). The inflammation (B) and steatosis (C) scores are reported. Moreover, the mRNA expression of proinflammatory parameters *Tlr4, Nfkb1*, *Ccl2, Emr1, Tnf*, *Il1b*, and *Il6* (D), is evaluated in the kidney of mice from all groups. Kidney ROS production was quantified, normalized to protein content, and expressed as a percentage of the control group mean (E). Gene expression of *Ppara (*F), *Fgf21* (G) and *Dgat1* (H). Results are shown as mean ± S.E.M (n=5–7 each group) (*P < 0,05, **P < 0,01, ***P < 0,001 and ****P < 0,0001).

3.5. OEA mitigates PAL-induced lipotoxicity in HK-2 cells

HK-2 cells were challenged with PAL in order to mimic the detrimental condition of renal lipotoxicity due to obesity. ORO staining revealed that the exposure to PAL led to a marked increase in cell lipid droplets (Fig. 6A). In contrast, OEA treatment significantly reduced lipid accumulation, as confirmed by the quantification of the relative ORO-stained area (Fig. 6B). Furthermore, PAL exposure resulted in a significant upregulation of key lipid metabolism markers, including *Fasn* (Fig. 6C) and *Cd36* (Fig. 6D), which are involved in lipid synthesis and uptake. However, OEA stimulation significantly attenuated the expression of both markers, suggesting its direct protective role against PAL-induced lipid dysregulation in renal cells.

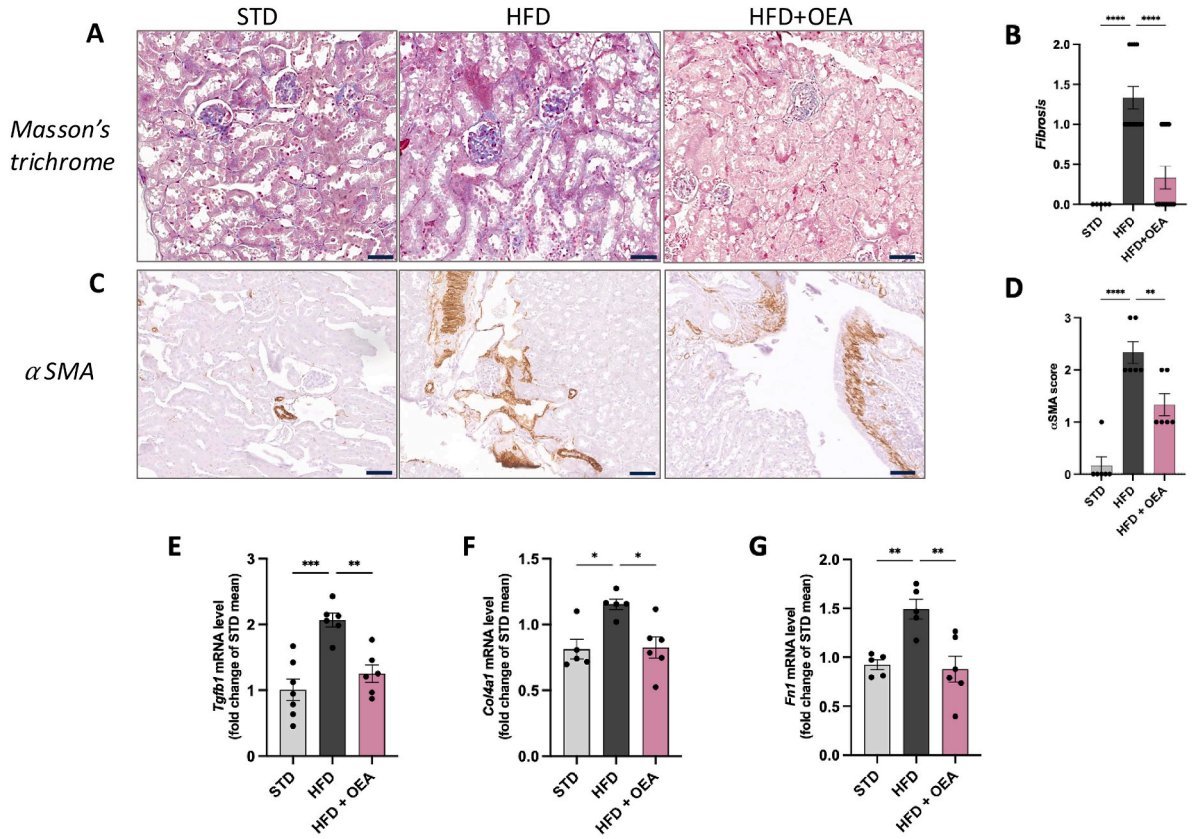

Fig. 5. OEA limits renal fibrotic responses in HFD-fed mice. Representative photomicrographs of Masson's trichrome-stained kidney sections (original magnification 200×) (A) and fibrosis score (B).
Representative photomicrographs of αSMA immunostained kidney section (C) and the corresponding scores (D). The gene expression of *Tgfb1* (E), *Col4a1* (F) and *Fn1* (G) is also assessed by RT-PCR in the kidney tissue. Results are shown as mean ± S.E.M (*P < 0,05, **P < 0,01 and ***P < 0,001).

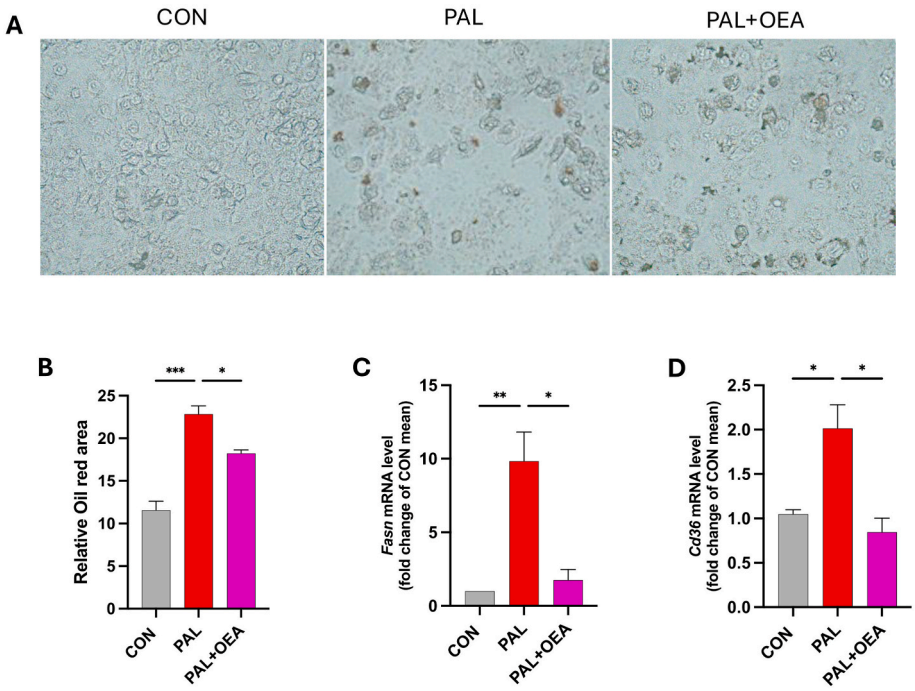

Fig. 6. OEA counteracts lipid dysmetabolism induced by PAL in HK-2 cells. PAL-challenged HK-2 cells, treated or not with PAL and OEA, are stained with ORO and observed under a light microscope (20× magnification) (A); the relative quantification of ORO area is also reported (B). The mRNA levels of *Fasn* (C) and *Cd36* (D) are measured. Results are shown as mean ± S.E.M of at least three independent experiments (*P < 0,05, **P < 0,01, ***P < 0,001).

3.6. OEA counteracts oxidative stress and mitochondrial dysfunction in PAL-challenged HK-2 cells

OEA antioxidant activity was assessed *in vitro* in PAL-stimulated HK-2 cells, demonstrating its ability in reducing ROS production (Fig. 7A). In the context of metabolic oxidative damage, mitochondria play a crucial role in cellular energy metabolism, generating the majority of intracellular adenosine triphosphate (ATP) through mitochondrial respiration (Gu et al., 2021). The Cell Mito Stress Test, a widely used assay for assessing key mitochondrial respiration parameters, was performed to evaluate the effect of OEA on mitochondrial bioenergetics in PAL-challenged cells (Fig. 7B). Notably, OEA stimulation increased basal respiration (Fig. 7C) and restored maximal respiration which was altered by PAL exposure (Fig. 7D). Moreover, OEA normalized proton leak (Fig. 7E), restored ATP-linked respiration (Fig. 7F), and enhanced spare respiratory capacity (Fig. 7G), which were impaired following PAL challenge. Collectively, these findings demonstrate that OEA directly counteracts PAL-induced mitochondrial dysfunction in renal cells.

4. Discussion

CKD is increasingly recognized as an escalating global health burden, with obesity identified as a major risk factor driving its onset and progression. HFD feeding and obesity trigger a cascade of metabolic derangements, including insulin resistance and ectopic fat deposition in various tissues including the kidney, where fat accumulation exacerbates lipotoxicity, oxidative stress and mitochondrial dysfunction, inflammation, and fibrosis. Given the increasing prevalence of obesity, recognized as an independent risk factor contributing to kidney injury, there is an urgent need for therapeutic strategies capable of counteracting the pathogenic mechanisms underlying renal injury secondary to metabolic dysfunction (Ruiz-Ortega et al., 2020). OEA, an endogenous lipid mediator known for its role in regulating appetite and energy balance (Sihag and Jones, 2018), has recently emerged as a promising compound with both metabolic and nephroprotective properties in the context of obesity-induced and acute-to-chronic kidney injury, respectively (Comella et al., 2024a, 2024b).

Here, we investigated OEA's protective effects in a mouse model of CKD induced by HFD feeding, focusing on its ability to mitigate metabolic alterations, inflammation, and fibrosis in the kidney. Notably, we highlight for the first time the dual role of OEA not only in controlling weight gain but also in exerting a significant nephroprotective effect against obesity-driven renal injury.

To date, OEA's beneficial effects are largely attributed to its activation of PPAR-α, a key regulator of lipid metabolism, which is abundantly expressed in the kidney and involved in maintaining energy balance (Gao and Gu, 2022; Ye et al., 2023). Beyond its metabolic functions, PPAR-α also exerts anti-inflammatory and antifibrotic effects, further supporting its potential implication in mitigating kidney damage associated with metabolic dysfunction (Tanaka et al., 2011; Xiong et al., 2024). In our experimental conditions, OEA firstly halts the increase in weight gain and fat mass of obese mice on HFD, reducing food intake (Supplementary data). These effects have been primarily attributed to the activation of PPAR-α, which accounts for the hypophagic activity, along with an increase in fatty acid metabolism and energy expenditure (Fu et al., 2003; Gaetani et al., 2010). Among other effects, long-term HFD feeding in mice resulted in significant kidney dysfunction, characterized by reduced water intake and urine output, elevated serum creatinine and BUN levels, and increased proteinuria, all hallmarks of renal impairment. It has been established that HFD feeding accelerates kidney damage, contributing to the onset of CKD (Li et al., 2021; Sun et al., 2020). However, OEA treatment effectively normalized these parameters, as well as markers of tubular injury such as KIM-1 and NGAL. The nephroprotective effect is particularly noteworthy given the established link between obesity-induced kidney injury and the accelerated progression to CKD.

Beyond its ability to counteract the overall metabolic dysregulation associated with obesity, as shown by systemic glucose and lipid profiles

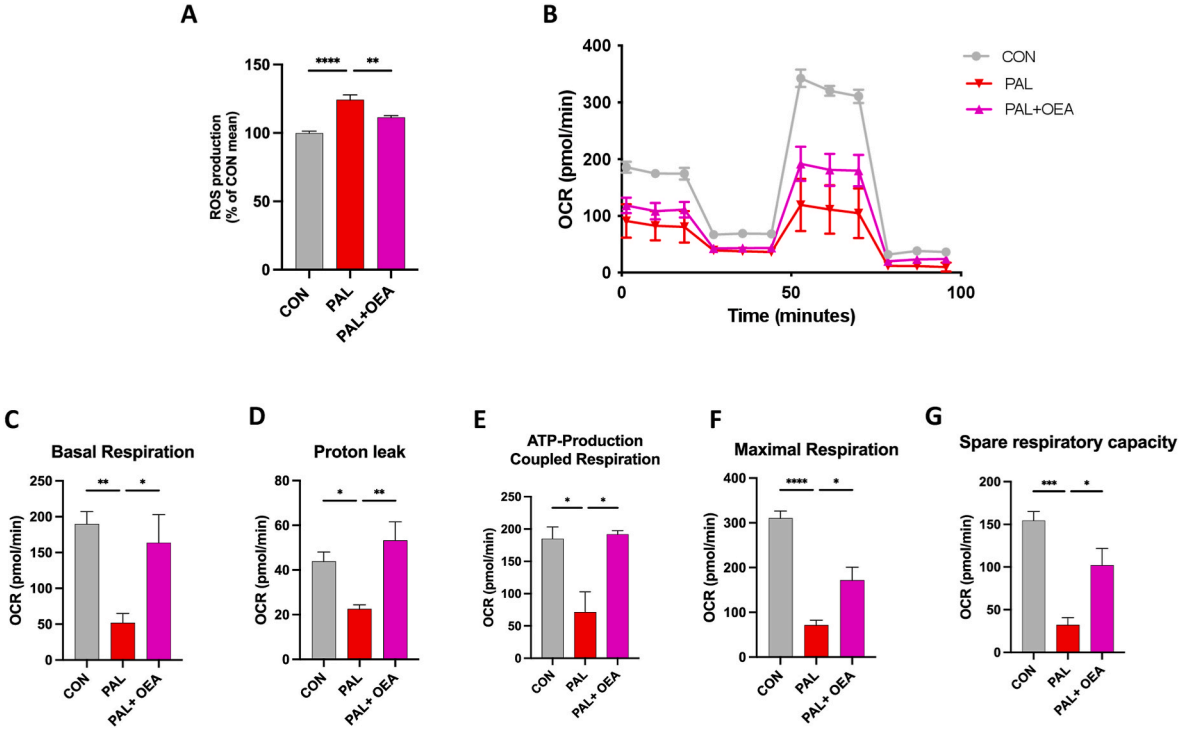

Fig. 7. OEA effects on ROS production and mitochondrial bioenergetics impaired by PAL in HK-2 cells. ROS accumulation was assessed in PAL-challenged HK-2 cells treated or not with OEA (A). Cell Mito Stress test is also performed using a Seahorse XFe24 analyzer (B). Specifically, basal respiration (C) proton leak (D), ATP-linked respiration (E), maximal respiration (F) and spare respiratory capacity (G) are assessed. Results are shown as mean ± S.E.M of at least three independent experiments (*P < 0,05, **P < 0,01, ***P < 0,001 and ****P < 0,0001).

(Supplementary data), OEA also demonstrated a renal-targeted metabolic effect, by improving HFD-altered renal glucose homeostasis. In fact, HFD feeding led to increased glycogen storage in the kidney of obese mice, alongside heightened gluconeogenesis, as shown by the upregulation of the enzyme PCK1. Additionally, we demonstrated an increased expression of glucose transporters such as GLUT2 and SGLT2, which are both implicated in renal glucose reabsorption (Jiang et al., 2019). Accordingly, knocking down the function of renal GLUT2 reverses hyperglycemia and normalizes body weight in obese and diabetic mice (de Souza Cordeiro et al., 2022). Notably, OEA treatment reduced the glycogen storage in renal tissue, lowering the transcription of PCK1 and improving the balance of glucose transporters by reduced protein expression. This, in turn, ameliorated the dysregulated glucose metabolism commonly associated with CKD, whether secondary or not to obesity.

Obesity-related lipid accumulation in peripheral organs, including the kidney, induces lipotoxicity, oxidative stress, inflammation, and fibrosis, ultimately leading to CKD (Rosenthal et al., 2020). Excessive levels of FFAs, triglycerides, and toxic lipid intermediates (e.g., ceramides, diacylglycerol) accumulate in renal tubular epithelial cells, podocytes, and mesangial cells, thereby activating pro-inflammatory and stress pathways. In the present study, the nephroprotective effects of OEA are particularly relevant given its role in lipid metabolism. As potent activator of PPAR-α, which is critical for regulating fatty acid oxidation in the kidney, OEA positively modulated PPAR-α signaling, likely contributing to a reduction in lipid accumulation in the kidney of HFD-fed mice. This is supported by the restored renal FGF21 expression, a PPAR-α-regulated factor that enhances fatty acid oxidation and energy homeostasis, and the decreased triglyceride trafficking, as indicated by the reduction of DGAT1 expression, which were altered in the kidney of obese mice. This dual regulation highlights OEA's ability to relieve renal lipid burden by promoting catabolic pathways and restraining anabolic ones. The decrease in lipid content was accompanied by a significant reduction in inflammatory markers, including IL-1β, IL-6, TNF-α, MCP-1, and F4/80, all of which were markedly upregulated in HFD-fed mice. Moreover, OEA treatment reduced the expression of TLR4 and NF-κB, both pivotal in initiating and propagating inflammatory and immune responses in the kidney. Collectively, these results indicate that OEA not only mitigates lipotoxicity but also exerts potent anti-inflammatory effects, likely through the involvement of PPAR-α, which plays a critical role in regulating both lipid metabolism and inflammatory responses (Chung et al., 2018; Impellizzeri et al., 2014).

Another key pathological feature of obesity-induced kidney injury is renal fibrosis, which plays a central role in CKD progression. Notably, Masson's trichrome staining, along with α-SMA immunohistochemical analysis, revealed OEA capability in limiting the fibrotic remodeling of kidney tissue caused by HFD feeding in mice, a crucial effect for preventing CKD progression. This latter finding was further corroborated by a reduction in the expression of fibrotic markers, e.g. TGF-β1, fibronectin, and collagen type IV. TGF-β1, a well-known mediator of renal fibrosis, is upregulation in obesity and has been implicated in CKD pathogenesis (Reiss et al., 2024). Indeed, the capability of OEA to attenuate TGF-β1 signaling and reduce extracellular matrix deposition underscores its antifibrotic properties, likely mediated through PPAR-α activation and its effects on lipid metabolism, inflammation, and oxidative stress (Comella et al., 2024b).

Lipotoxicity and renal fibrosis are closely linked with oxidative damage and mitochondrial dysfunction, all processes that collectively contribute to the pathogenesis and progression of CKD. Their interplay represents a key pathway in kidney injury, particularly in metabolic disorders, such as obesity and diabetes (Xu et al., 2024). In fact, excessive lipid flux can overwhelm mitochondrial capacity, resulting in compromised fatty acid β-oxidation and accumulation of toxic intermediates (Ge et al., 2020). Mitochondrial dysfunction, another hallmark of obesity-related kidney injury, further exacerbates impaired energy metabolism and renal cell damage (Lumpuy-Castillo et al., 2024). Since mitochondrial damage represents a major source of oxidative stress in obesity, we measured total ROS amount in both kidney and HK-2 cells as an indirect but reliable proxy of altered mitochondrial redox balance, consistently with other findings (Gwon et al., 2017; Sun et al., 2020). Indeed, numerous studies (Bournat and Brown, 2010; Chouchani et al., 2016, 2017; Handy and Loscalzo, 2012) have demonstrated that mitochondrial electron transport chain dysfunction accounts for the vast majority of ROS generated under metabolic stress conditions, far exceeding the contribution of other cellular sources.

Our results show that ROS levels were markedly elevated in the kidney of HFD mice as well as palmitate-challenged tubular cells, as a cellular model of lipotoxicity, compared with relative controls, whereas OEA treatment significantly reduced ROS accumulation both *in vivo* than *in vitro*, indicating a direct nephroprotective effect against obesity-induced oxidative stress and mitochondrial impairment.

Delving into mitochondrial bioenergetics, we performed the Mito-Stress test using SeaHorse analyzer in palmitate-challenged HK-2 tubular cells. Here, we found that OEA treatment improved mitochondrial function. Specifically, OEA restored key parameters of mitochondrial respiration, proton leak including basal respiration, maximal respiration, ATP-linked respiration, and spare respiratory capacity. These findings indicate that OEA exerts a direct protective effect on mitochondrial bioenergetics, potentially mitigating the energy deficits underlying renal cell dysfunction, inflammation, and fibrosis in obesity-related kidney injury. It is well-established that lipid overload-induced mitochondrial stress generates an excessive production of ROS, leading to oxidative damage. In obesity, the loss of mitochondrial membrane potential disrupts ATP production, ultimately leading to energy depletion in metabolically active renal cells (Permyakova et al., 2024; Srivastava et al., 2020). Finally, damaged mitochondria release pro-apoptotic factors (e.g., cytochrome *c*) and damage-associated molecular patterns (DAMPs), amplifying cellular injury. Moreover, using an *in vitro* model of renal damage by palmitate, we have further assessed the direct effect of OEA on epithelial tubular cells in counteracting lipotoxicity. Previous studies have explored the mechanisms underlying PAL-induced lipid deposition and following lipotoxicity in HK-2 cells, indicating the involvement of fatty acid oxidation (FAO)-regulating proteins (e.g. PPAR-α and CPT-1 (Sun et al., 2018) or lipid anabolism- and catabolism-associated genes (Wu et al., 2019). Here, we showed a decrease of cell lipid accumulation by ORO staining strictly associated with reduced FAS and CD36 transcription in OEA-treated PAL-challenged cells. Among all, FAS is a key enzyme responsible for the *de novo* synthesis of fatty acids, catalyzing the final steps in fatty acid production. FAS plays an essential role in lipid metabolism, particularly under conditions of overnutrition or excessive calorie intake, such as during obesity. In this context, FAS contributes to the accumulation of excess lipids, which can lead to harmful effects such as lipotoxicity, tissue fibrosis, and the onset or development of obesity-related diseases, including CKD (Kume et al., 2007; Li and Humphreys, 2024; Mount et al., 2015; Szolkiewicz et al., 2002).

Taken together, our findings demonstrate that OEA exerts a dual action in protecting against obesity-induced CKD. By regulating lipid metabolism, OEA not only prevents obesity and weight gain but also reduces renal lipotoxicity, and associated inflammation, fibrosis, and mitochondrial dysfunction. These combined effects converge in improved kidney function and attenuation of CKD progression in obese mice. Given the rising global prevalence of obesity and its strong association with CKD, OEA represents a promising dual-action therapeutic candidate for managing both metabolic disturbances and renal dysfunction in patients with obesity at risk of related kidney disease. The translational potential of OEA appears particularly compelling within an integrative therapeutic framework, where it could be used alongside current pharmacological treatments. Rather than serving as a standalone agent, OEA may function as an adjunct therapy, a strategy that could enhance both its clinical feasibility and its relevance in human settings. Further studies are warranted to investigate the clinical

potential of OEA in human obesity-related CKD and to explore its broader applications in other forms of metabolic kidney disease.

Limitations of the study

This study presents some limitations that should be acknowledged. First, while our findings suggest potential direct mechanisms underlying OEA's protective effects on the kidney, mechanistic insights were not reported, as the direct involvement of PPAR-α in mediating OEA's renoprotective effects has already been demonstrated in a recent publication by our group using another model of kidney injury (Comella et al., 2024b). Indeed, this study demonstrated the mechanistic role of PPAR-α activation in driving OEA's nephroprotective profile, targeting key pathological features shared with obesity-related CKD, including renal inflammation, lipid accumulation, and fibrosis. Another limitation of our study is the exclusive use of male mice. While this choice was made to avoid potential confounding effects of hormonal fluctuations and to specifically address the renoprotective action of OEA in obesity-induced CKD, future studies should evaluate sex-specific responses to better capture the translational impact of OEA.

CRediT authorship contribution statement

Federica Comella: Writing – original draft, Investigation, Data curation. **Stefania Melini:** Investigation, Data curation. **Nicola Opallo:** Investigation, Data curation. **Evaristo Di Napoli:** Investigation, Data curation. **Nicole Pia Navatti:** Investigation, Data curation. **Orlando Paciello:** Validation, Data curation. **Maria Carmela Ferrante:** Visualization, Validation. **Rosaria Meli:** Supervision, Data curation, Conceptualization. **Giuseppina Mattace Raso:** Writing – original draft, Supervision, Methodology, Data curation, Conceptualization. **Claudio Pirozzi:** Writing – original draft, Supervision, Methodology, Data curation, Conceptualization.

Funding

This work was partially supported by a grant from POC R&I 2014–2020, Asse tematico I "Capitale Umano"- Azione I.1 "Dottorati innovative con caratterizzazione industriale".

Declaration of competing interest

Nothing to declare.

Acknowledgments

We thank Mr Giovanni Esposito, Mr Angelo Russo and Dr Antonio Baiano for animal care and technical assistance.

Appendix A. Supplementary data

Supplementary data to this article can be found online at https://doi.org/10.1016/j.ejphar.2025.178436.

Data availability

Data will be made available on request.

References

Bournat, J.C., Brown, C.W., 2010. Mitochondrial dysfunction in obesity. Curr. Opin. Endocrinol. Diabetes Obes. 17, 446–452.
Brand, M.D., Nicholls, D.G., 2011. Assessing mitochondrial dysfunction in cells. Biochem. J. 435, 297–312.
Chen, L., Li, L., Chen, J., Li, L., Zheng, Z., Ren, J., Qiu, Y., 2015. Oleoylethanolamide, an endogenous PPAR-alpha ligand, attenuates liver fibrosis targeting hepatic stellate cells. Oncotarget 6, 42530–42540.
Chouchani, E.T., Kazak, L., Jedrychowski, M.P., Lu, G.Z., Erickson, B.K., Szpyt, J., Pierce, K.A., Laznik-Bogoslavski, D., Vetrivelan, R., Clish, C.B., Robinson, A.J., Gygi, S.P., Spiegelman, B.M., 2016. Mitochondrial ROS regulate thermogenic energy expenditure and sulfenylation of UCP1. Nature 532, 112–116.
Chouchani, E.T., Kazak, L., Spiegelman, B.M., 2017. Mitochondrial reactive oxygen species and adipose tissue thermogenesis: bridging physiology and mechanisms. J. Biol. Chem. 292, 16810–16816.
Chung, K.W., Lee, E.K., Lee, M.K., Oh, G.T., Yu, B.P., Chung, H.Y., 2018. Impairment of PPARalpha and the Fatty acid oxidation pathway aggravates renal fibrosis during aging. J. Am. Soc. Nephrol. 29, 1223–1237.
Comella, F., Aragon-Herrera, A., Pirozzi, C., Feijoo-Bandin, S., Lama, A., Opallo, N., Melini, S., Del Piano, F., Gualillo, O., Meli, R., Mattace Raso, G., Lago, F., 2024a. Oleoylethanolamide mitigates cardiometabolic disruption secondary to obesity induced by high-fat diet in mice. Life Sci. 359, 123226.
Comella, F., Lama, A., Pirozzi, C., Annunziata, C., Piegari, G., Sodano, F., Melini, S., Paciello, O., Lago Paz, F., Meli, R., Mattace Raso, G., 2024b. Oleoylethanolamide attenuates acute-to-chronic kidney injury: in vivo and in vitro evidence of PPAR-alpha involvement. Biomed. Pharmacother. 171, 116094.
De Biase, D., De Leo, M., Piegari, G., d'Aquino, I., Di Napoli, E., Mercogliano, C., Calabria, A., Pula, A., Navas, L., Russo, V., Paciello, O., 2024. Investigation of the theragnostic role of KIT expression for the treatment of canine mast cell tumors with tyrosine kinase inhibitors. Vet. Sci. 11.
de Souza Cordeiro, L.M., Bainbridge, L., Devisetty, N., McDougal, D.H., Peters, D.J.M., Chhabra, K.H., 2022. Loss of function of renal Glut2 reverses hyperglycaemia and normalises body weight in mouse models of diabetes and obesity. Diabetologia 65, 1032–1047.
Dimatteo, M., Di Napoli, E., Paciello, O., d'Aquino, I., Iaccarino, D., D'Amore, M., Guida, M., Cozzolino, L., Serpe, F.P., Fusco, G., De Carlo, E., Degli Uberti, B., 2024. Pathological changes and CYP1A1 expression as biomarkers of pollution in Sarpa Salpa and diplodus sargus. Animals (Basel) 14.
Dranka, B.P., Benavides, G.A., Diers, A.R., Giordano, S., Zelickson, B.R., Reily, C., Zou, L., Chatham, J.C., Hill, B.G., Zhang, J., Landar, A., Darley-Usmar, V.M., 2011. Assessing bioenergetic function in response to oxidative stress by metabolic profiling. Free Radic. Biol. Med. 51, 1621–1635.
Francis, A., Harhay, M.N., Ong, A.C.M., Tummalapalli, S.L., Ortiz, A., Fogo, A.B., Fliser, D., Roy-Chaudhury, P., Fontana, M., Nangaku, M., Wanner, C., Malik, C., Hradsky, A., Adu, D., Bavanandan, S., Cusumano, A., Sola, L., Ulasi, I., Jha, V., American Society of, N., European Renal, A., International Society of, N., 2024. Chronic kidney disease and the global public health agenda: an international consensus. Nat. Rev. Nephrol. 20, 473–485.
Freireich, E.J., Gehan, E.A., Rall, D.P., Schmidt, L.H., Skipper, H.E., 1966. Quantitative comparison of toxicity of anticancer agents in mouse, rat, hamster, dog, monkey, and man. Cancer Chemother. Rep. 50, 219–244.
Fu, J., Gaetani, S., Oveisi, F., Lo Verme, J., Serrano, A., Rodriguez De Fonseca, F., Rosengarth, A., Luecke, H., Di Giacomo, B., Tarzia, G., Piomelli, D., 2003. Oleylethanolamide regulates feeding and body weight through activation of the nuclear receptor PPAR-alpha. Nature 425, 90–93.
Gaetani, S., Fu, J., Cassano, T., Dipasquale, P., Romano, A., Righetti, L., Cianci, S., Laconca, L., Giannini, E., Scaccianoce, S., Mairesse, J., Cuomo, V., Piomelli, D., 2010. The fat-induced satiety factor oleoylethanolamide suppresses feeding through central release of oxytocin. J. Neurosci. 30, 8096–8101.
Gao, J., Gu, Z., 2022. The role of peroxisome proliferator-activated receptors in kidney diseases. Front. Pharmacol. 13, 832732.
Ge, M., Fontanesi, F., Merscher, S., Fornoni, A., 2020. The vicious cycle of renal lipotoxicity and mitochondrial dysfunction. Front. Physiol. 11, 732.
Gu, X., Ma, Y., Liu, Y., Wan, Q., 2021. Measurement of mitochondrial respiration in adherent cells by Seahorse XF96 Cell Mito Stress Test. STAR Protoc. 2, 100245.
Guan, Y., 2002. Targeting peroxisome proliferator-activated receptors (PPARs) in kidney and urologic disease. Minerva Urol. Nefrol. 54, 65–79.
Gwon, D.H., Hwang, T.W., Ro, J.Y., Kang, Y.J., Jeong, J.Y., Kim, D.K., Lim, K., Kim, D. W., Choi, D.E., Kim, J.J., 2017. High endogenous accumulation of omega-3 polyunsaturated Fatty acids protect against ischemia-reperfusion renal injury through AMPK-Mediated autophagy in Fat-1 mice. Int. J. Mol. Sci. 18.
Handy, D.E., Loscalzo, J., 2012. Redox regulation of mitochondrial function. Antioxidants Redox Signal. 16, 1323–1367.
Impellizzeri, D., Esposito, E., Attley, J., Cuzzocrea, S., 2014. Targeting inflammation: new therapeutic approaches in chronic kidney disease (CKD). Pharmacol. Res. 81, 91–102.
Jiang, Y.K., Xin, K.Y., Ge, H.W., Kong, F.J., Zhao, G., 2019. Upregulation of renal GLUT2 and SGLT2 is involved in high-fat diet-induced gestational diabetes in mice. Diabetes Metab Syndr Obes 12, 2095–2105.
Kalantar-Zadeh, K., Li, P.K., 2020. Strategies to prevent kidney disease and its progression. Nat. Rev. Nephrol. 16, 129–130.
Kamijo, Y., Hora, K., Tanaka, N., Usuda, N., Kiyosawa, K., Nakajima, T., Gonzalez, F.J., Aoyama, T., 2002. Identification of functions of peroxisome proliferator-activated receptor alpha in proximal tubules. J. Am. Soc. Nephrol. 13, 1691–1702.
Kounatidis, D., Vallianou, N.G., Stratigou, T., Voukali, M., Karampela, I., Dalamaga, M., 2024. The kidney in obesity: current evidence, perspectives and controversies. Curr Obes Rep 13, 680–702.
Kume, S., Uzu, T., Araki, S., Sugimoto, T., Isshiki, K., Chin-Kanasaki, M., Sakaguchi, M., Kubota, N., Terauchi, Y., Kadowaki, T., Haneda, M., Kashiwagi, A., Koya, D., 2007. Role of altered renal lipid metabolism in the development of renal injury induced by a high-fat diet. J. Am. Soc. Nephrol. 18, 2715–2723.
Laleh, P., Yaser, K., Abolfazl, B., Shahriar, A., Mohammad, A.J., Nazila, F., Alireza, O., 2018. Oleoylethanolamide increases the expression of PPAR-Alpha and reduces appetite and body weight in obese people: a clinical trial. Appetite 128, 44–49.

Lee, L.E., Doke, T., Mukhi, D., Susztak, K., 2024. The key role of altered tubule cell lipid metabolism in kidney disease development. Kidney Int. 106, 24–34.
Li, H., Humphreys, B.D., 2024. Targeting de novo lipogenesis to mitigate kidney disease. J. Clin. Investig. 134.
Li, Q., Ge, C., Tan, J., Sun, Y., Kuang, Q., Dai, X., Zhong, S., Yi, C., Hu, L.F., Lou, D.S., Xu, M., 2021. Juglanin protects against high fat diet-induced renal injury by suppressing inflammation and dyslipidemia via regulating NF-kappaB/HDAC3 signaling. Int. Immunopharmacol. 95, 107340.
Li, S., Nagothu, K.K., Desai, V., Lee, T., Branham, W., Moland, C., Megyesi, J.K., Crew, M. D., Portilla, D., 2009. Transgenic expression of proximal tubule peroxisome proliferator-activated receptor-alpha in mice confers protection during acute kidney injury. Kidney Int. 76, 1049–1062.
Lumpuy-Castillo, J., Amador-Martinez, I., Diaz-Rojas, M., Lorenzo, O., Pedraza-Chaverri, J., Sanchez-Lozada, L.G., Aparicio-Trejo, O.E., 2024. Role of mitochondria in reno-cardiac diseases: a study of bioenergetics, biogenesis, and GSH signaling in disease transition. Redox Biol. 76, 103340.
Mattace Raso, G., Simeoli, R., Russo, R., Santoro, A., Pirozzi, C., d'Emmanuele di Villa Bianca, R., Mitidieri, E., Paciello, O., Pagano, T.B., Orefice, N.S., Meli, R., Calignano, A., 2013. N-Palmitoylethanolamide protects the kidney from hypertensive injury in spontaneously hypertensive rats via inhibition of oxidative stress. Pharmacol. Res. 76, 67–76.
Mount, P., Davies, M., Choy, S.W., Cook, N., Power, D., 2015. Obesity-Related chronic kidney disease-the role of lipid metabolism. Metabolites 5, 720–732.
Park, C.W., Kim, H.W., Ko, S.H., Chung, H.W., Lim, S.W., Yang, C.W., Chang, Y.S., Sugawara, A., Guan, Y., Breyer, M.D., 2006. Accelerated diabetic nephropathy in mice lacking the peroxisome proliferator-activated receptor alpha. Diabetes 55, 885–893.
Permyakova, A., Hamad, S., Hinden, L., Baraghithy, S., Kogot-Levin, A., Yosef, O., Shalev, O., Tripathi, M.K., Amal, H., Basu, A., Arif, M., Cinar, R., Kunos, G., Berger, M., Leibowitz, G., Tam, J., 2024. Renal mitochondrial ATP transporter ablation ameliorates obesity-induced CKD. J. Am. Soc. Nephrol. 35, 281–298.
Pirozzi, C., Lama, A., Annunziata, C., Cavaliere, G., De Caro, C., Citraro, R., Russo, E., Tallarico, M., Iannone, M., Ferrante, M.C., Mollica, M.P., Mattace Raso, G., De Sarro, G., Calignano, A., Meli, R., 2020. Butyrate prevents valproate-induced liver injury: in vitro and in vivo evidence. FASEB J. 34, 676–690.
Pontis, S., Ribeiro, A., Sasso, O., Piomelli, D., 2016. Macrophage-derived lipid agonists of PPAR-alpha as intrinsic controllers of inflammation. Crit. Rev. Biochem. Mol. Biol. 51, 7–14.
Reiss, A.B., Jacob, B., Zubair, A., Srivastava, A., Johnson, M., De Leon, J., 2024. Fibrosis in chronic kidney disease: pathophysiology and therapeutic targets. J. Clin. Med. 13.
Ren, L., Cui, H., Wang, Y., Ju, F., Cai, Y., Gang, X., Wang, G., 2023. The role of lipotoxicity in kidney disease: from molecular mechanisms to therapeutic prospects. Biomed. Pharmacother. 161, 114465.
Rosenthal, T.R., Park, S.K., Kairamkonda, S., Khatoon, S., Pop, L.M., Bobulescu, I.A., 2020. Renal lipid accumulation, oxidative stress and uric acid handling in a rodent model of obesity and metabolic syndrome. J Investig Med.
Ruggiero, C., Ehrenshaft, M., Cleland, E., Stadler, K., 2011. High-fat diet induces an initial adaptation of mitochondrial bioenergetics in the kidney despite evident oxidative stress and mitochondrial ROS production. Am. J. Physiol. Endocrinol. Metab. 300, E1047–E1058.
Ruiz-Ortega, M., Rayego-Mateos, S., Lamas, S., Ortiz, A., Rodrigues-Diez, R.R., 2020. Targeting the progression of chronic kidney disease. Nat. Rev. Nephrol. 16, 269–288.
Sihag, J., Jones, P.J.H., 2018. Oleoylethanolamide: the role of a bioactive lipid amide in modulating eating behaviour. Obes. Rev. 19, 178–197.
Srivastava, S.P., Kanasaki, K., Goodwin, J.E., 2020. Loss of mitochondrial control impacts renal health. Front. Pharmacol. 11, 543973.
Sun, J., Chen, X., Liu, T., Jiang, X., Wu, Y., Yang, S., Hua, W., Li, Z., Huang, H., Ruan, X., Du, X., 2018. Berberine protects against palmitate-induced apoptosis in tubular epithelial cells by promoting fatty acid oxidation. Med. Sci. Monit. 24, 1484–1492.
Sun, Y., Ge, X., Li, X., He, J., Wei, X., Du, J., Sun, J., Li, X., Xun, Z., Liu, W., Zhang, H., Wang, Z.Y., Li, Y.C., 2020. High-fat diet promotes renal injury by inducing oxidative stress and mitochondrial dysfunction. Cell Death Dis. 11, 914.
Szolkiewicz, M., Nieweglowski, T., Korczynska, J., Sucajtys, E., Stelmanska, E., Goyke, E., Swierczynski, J., Rutkowski, B., 2002. Upregulation of fatty acid synthase gene expression in experimental chronic renal failure. Metabolism 51, 1605–1610.
Taber-Hight, E., Gilmore, A., Friedman, A.N., 2024. Anti-obesity pharmacotherapy in adults with chronic kidney disease. Kidney Int. 105, 269–280.
Tanaka, Y., Kume, S., Araki, S., Isshiki, K., Chin-Kanasaki, M., Sakaguchi, M., Sugimoto, T., Koya, D., Haneda, M., Kashiwagi, A., Maegawa, H., Uzu, T., 2011. Fenofibrate, a PPARalpha agonist, has renoprotective effects in mice by enhancing renal lipolysis. Kidney Int. 79, 871–882.
Vaccaro, E., Navas, L., Ercolano, M., Piegari, G., Di Napoli, E., Papparella, S., Inverso, D., Brunetti, B., Paciello, O., Russo, V., 2024. Immunohistochemical investigation of Cyclooxygenase-2 expression in rabbit uterine adenocarcinoma and the potential use of COX-2 inhibitors in cancer therapy. Animals (Basel) 14.
Verissimo, T., Dalga, D., Arnoux, G., Sakhi, I., Faivre, A., Auwerx, H., Bourgeois, S., Paolucci, D., Gex, Q., Rutkowski, J.M., Legouis, D., Wagner, C.A., Hall, A.M., de Seigneux, S., 2023. PCK1 is a key regulator of metabolic and mitochondrial functions in renal tubular cells. Am. J. Physiol. Ren. Physiol. 324, F532–F543.
Wei, P., Lane, P.H., Lane, J.T., Padanilam, B.J., Sansom, S.C., 2004. Glomerular structural and functional changes in a high-fat diet mouse model of early-stage Type 2 diabetes. Diabetologia 47, 1541–1549.
Wu, Y., Chen, F., Huang, X., Zhang, R., Yu, Z., Chen, Z., Liu, J., 2019. Berberine (BBR) attenuated palmitic acid (PA)-Induced lipotoxicity in human HK-2 cells by promoting peroxisome proliferator-activated receptor alpha (PPAR-alpha). Med. Sci. Monit. 25, 7702–7708.
Xiong, Y., Zhong, J., Chen, W., Li, X., Liu, H., Li, Y., Xiong, W., Li, H., 2024. Neferine alleviates acute kidney injury by regulating the PPAR-alpha/NF-kappaB pathway. Clin. Exp. Nephrol. 28, 969–987.
Xu, W., Zhu, Y., Wang, S., Liu, J., Li, H., 2024. From adipose to ailing kidneys: the role of lipid metabolism in obesity-related chronic kidney disease. Antioxidants 13.
Yang, F.J., He, Y.H., Zhou, J.H., 2015. Fenofibrate pre-treatment suppressed inflammation by activating phosphoinositide 3 kinase/protein kinase B (PI3K/Akt) signaling in renal ischemia-reperfusion injury. J Huazhong Univ Sci Technolog Med Sci 35, 58–63.
Ye, M., Yang, M., Dai, W., Li, H., Zhou, X., Chen, Y., He, L., 2023. Targeting renal proximal tubule cells in obesity-related glomerulopathy. Pharmaceuticals 16.